Available online at www.sciencedirect.com

ScienceDirect

Procedia CIRP 102 (2021) 222–227

www.elsevier.com/locate/procedia

18th CIRP Conference on Modeling of Machining Operations

Modeling of cutting force in micro-end-milling process with experimental validation on additive manufactured Nickel-based superalloy

Andrea Abeni[a]*, Dario Loda[a,b], Tuğrul Özel[b], Aldo Attanasio[a]

[a]*University of Brescia, Via Branze 38, 25123 Brescia, Italy*
[b]*Rutgers University, Industrial & Systems Engineering, Piscataway, New Jersey, USA*

* Corresponding author. Tel.: +39 030 3715584. *E-mail address:* andrea.abeni@unibs.it

Abstract

Nowadays aerospace, microelectronics, biotechnology industries require small sized components with complex shape and high mechanical properties, often operating in aggressive environment. In this framework, Additive Manufacturing (AM) of Nickel-based superalloys is an interesting and cost effective process. Fewer design constraints and the weight reduction achievable through the topology optimization are the most relevant AM advantages. Furthermore, micro-scale features on the additively fabricated parts can be manufactured by using micro machining. Subtractive processes ensure to achieve high-precision mechanical coupling due to better surface finishes and tighter tolerances. A lack of scientific studies focusses on the material removal behavior of difficulty-to-cut alloys produced via Additive Manufacturing is evident. This work describes a machining analytical force models which considers the presence of ploughing- and shearing- dominated cutting regimes. The undefined cutting force model parameters and the Minimum Uncut Chip Thickness (MUCT) can be identified through proper experimental tests. The refinement procedure of the model was utilized to characterize Inconel 625 samples fabricated by LaserCUSING^{TM}. The cutting force data were elaborated with an iterative methodology based on a search algorithm. The model successfully predicted how the cutting force changes as a function of the process parameters.

Keywords: Analytical model; Micro machining; Inconel 625; MUCT; Cutting force

1. Introduction

The Nickel-based superalloys are a class of metal alloys characterized by remarkable thermo-mechanical proprieties. High strength, high corrosion resistance, super-elasticity behavior, elevated wear resistance and high temperature strengths are the most attractive features of the Nickel-based superalloys [1]. The trademark “Inconel” designates a specific class of Nickel-based alloys utilized in extreme environments. The parts and the components made by Inconel are usually formed by conventional processes, such as casting and hot plastic deformation. Moreover, machining processes are utilized to manufacture complex three-dimensional features and to improve the surface finishing. Inconel is a hard-to-cut material, due to the strain hardening effect and the thermal stability [2]. In the last years, an increasing number of products in Inconel have been manufactured through Additive Manufacturing (AM), especially in aerospace industry [3]. A more flexibility in design, the rapidity in prototyping and the minimizing of material waste are the most established AM advantages [4]. The main drawbacks of additively manufactured metal products are the high surface roughness combined with the larger dimensional tolerances if compared with machining. In this context, a combination between AM

10.1016/j.procir.2021.09.038

and conventional subtractive process appears profitable. Miniaturized features and surface finishing could be manufactured through machining on rough products fabricated in Inconel by AM.

The machining of difficult-to-cut materials is affected by increasing issues as the tool size decreases. Burr formation, rapid tool wear, high cutting force, tool run-out effects are the most relevant consequence of the size reduction in cutting [5]. The investigation of the material behavior in micro machining is a fundamental topic which requires time consuming and costly experimental tests. Among the experimental output, cutting force is generally considered a fundamental magnitude to understand and control the process [6]. Several researches have deepened the phenomena which influence the contact between the tool and the workpiece in micro machining, such as the high strain rate effect, the heat generation in localized material zone and the elastic recovering effect [7, 8 and 9]. The studies have resulted in different cutting models with the common aim of accurately predicting the cutting forces. Kuram and Ozcelik [10] elaborated an empirical model by fitting experimental data capable of predicting tool wear, surface roughness and cutting forces in micro-milling of Inconel 718. The limitations of empirical models favorited the wide spread of analytical formulation based on theoretical approach. Budak et al. [11] proposed an analytical model able to predict stagnation zones and edge cutting forces in primary, secondary and third deformation zones. The tool deflection effect on cutting force was computed in the model elaborated by Moges et al. [12]. The phenomenon influences the actual tool trajectories and it determines a modification of the uncut chip thickness. In micromachining, the chip thickness has a meaningful impact on the material removal mechanism. If the actual chip thickness is lower than the Minimum Uncut Chip Thickness (MUCT), a ridge of material is ploughed and pushed ahead of tool cutting edge without chip formation [13]. The integrity of the machined surface and the cutting force are strongly influenced by ploughing [14]. The phenomena should be considered in a cutting model for micro machining. Rodriguez and Labarga [15] considered MUCT to define the entry and the exit angles of the end-milling tool in shear cutting regime. The cutting force were computed by considering size effect, tool run-out and deflection. Chen et al. [16] calculated the cutting force by considering the alternance between ploughing and shearing as a function of the uncut chip thickness. A higher accuracy in cutting force prediction was demonstrated by a comparison with conventional model in different cutting condition. A similar achievement was obtained by Zhang et al. [17] with a three dimensional cutting force model that includes the effect of ploughing as function of the cutting edge radius.

In this study, a cutting force model [21] was improved and optimized for a specific grade of Additively Manufactured Ni-Cr-Mo superalloy, named Inconel 625. A new objective function was defined, and the outputs were compared with the results of the original version of the model. The model can be applied also to others AM or conventionally formed materials, in order to successfully predict cutting force in micro milling. A geometrical model was elaborated in order to consider the concomitant presence of ploughing and shearing and how the prevalence of one of them on the other changes during a single tool rotation. Experimental micro milling tests were appositely designed and executed to calculate MUCT firstly and to subsequently calibrate the model.

2. Materials and Methods

Micro milling of AM Inconel 625 was performed by using the ultra-precision 5 axes machining center Kern Pyramid Nano (precision of ±0.3 µm). The samples were fabricated via L-PBF process, by using GE Additive Concept Laser M2 Cusing machine. The angle chosen for the laser building strategy was 0° in relation to the building plate. The powder particle size was ranging between 15 µm and 45 µm. The samples were not heat treated or hot isostatically pressed. Table 1 summarizes the laser power P, the scan velocity vs, the laser spot size d, the layer thickness s, the hatch distance h, the stripe width w and volumetric energy density E.

Table 1. The process parameters of L-PBF on Inconel 625.

P (W)	v_s (mm/s)	d (µm)	s (µm)	h (µm)	w (mm)	E (J/mm^3)
370	1200	170	60	110	5	46.7

The sample shapes were designed in order to constrain the samples on a piezoelectric 3-component loadcell (Kistler 9317C, shown in Fig. 1). The force measuring system accuracy is equal to 0.1 N, the sampling rate is 50 kHz and the natural frequency is higher than the tooth path frequency [18]. A low pass filter with a cut off frequency equal to 2000 KHz was adopted. Cutting was performed in dry condition orienting the mill axis as the sample building direction.

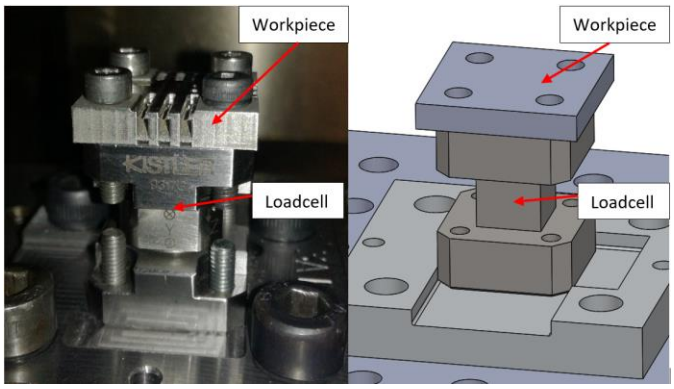

(a) **(b)**

Fig. 1. (a) Inconel 625 workpiece mounted on the loadcell; (b) 3D CAD of the sample

Experimental tests can be divided into two groups. Preliminary micro slots machining was performed to calculate the MUCT, while full immersion micro-machining allowed to calibrate the analytical model. The first slots were machined on a parallelepiped shape sample, while the second group of tests were performed on a thin-walled sample. Two different micro end mills were employed. A 3D digital microscope allowed to measure the actual tool dimensions for both mills. Table 2 summarizes the main features of the tool utilized for the MUCT

tests (SECO 905) and the tool employed for the model calibration tests (SECO 103).

For the MUCT estimation, a standard micro mill (SECO 905) was used with the aim of representing standard cutting conditions. Twenty slots were fabricated with a constant depth of cut equal to 200 µm, by using a constant cutting speed of 40 m/min. The feed per tooth f_z was increased from 0.5 µm/rev*tooth to a maximum of 10 µm/rev*tooth, with an increment of 0.5 µm.

Table 2. The main features of the SECO micro end mills.

Micro mill code	SECO 905L008-MEGA-T	SECO 103L008-MEGA-64T
Nominal diameter (µm)	800	800
Effective diameter (µm)	791 ±1	789 ± 3
Measured cutting edge radius (µm)	5	4
Helix angle (°)	20	0
Rake angle (°)	4	0
Material	Tungsten Carbide	Tungsten Carbide
Material coating	Titanium Nitride	Titanium Nitride

The second group of experimental tests consists in thin-wall channel-milling performed in semi-orthogonal cutting condition. This set-up was obtained using micro mill with a helix angle of 0° (SECO 103) [19]. Feed rate was varied on three levels, while two cutting speeds were tested. Table 3 shows the process parameters utilized.

Table 3. Process parameters of micro milling of thin-walls.

Test	Feed per tooth (µm/rev*tooth)	Cutting speed (m/min)
1	2.5	30
2	2.5	40
3	5	30
4	5	40
5	10	30
6	10	40

Each thin-wall thickness was measured in order to calculate the depth of cut. It averagely resulted equal to 171± 17 µm. Since the thin-walls on the samples were fabricated via AM, the accuracy about the thickness is limited. Moreover, the effective value of thickness of each slot was utilized in the analytical model calibration procedure. Each test was repeated three times to statistically validate the analytical model.

3. Analytical force model

The analytical model is suitable to predict the cutting force for two-dimensional micro milling of slots on thin-walled samples with a 2-flutes, zero-degree rake angle and zero-degree helix angle end-mill.

Fig. 2 illustrates the geometrical model and the cutting force F_c decomposition in the tangential component (F_t) and the radial component (F_r) and in the cartesian components F_x and F_y. Further details about the model developed by the authors can be found in [21].

For small feed rate the instantaneous value of the thickness t_u can be expressed by Eq. 1:

$$t_u(\theta) = f_z * sin(\omega * t) = f_z * sin(\theta) \quad (1)$$

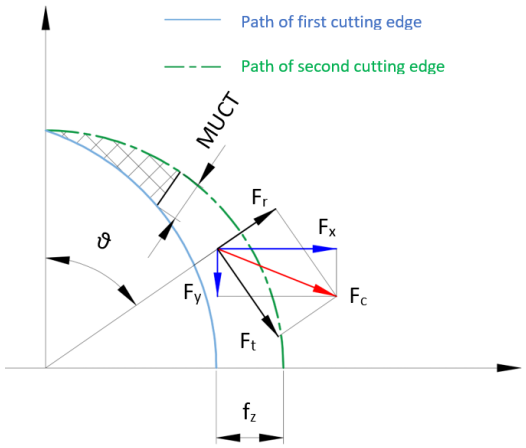

Fig. 2. Schematization of slot milling.

Since the uncut chip thickness ranges from zero to f_z, the ploughing phenomenon inevitably characterizes micro slot machining. Ploughing is the unique cutting regime for t_u ranging from zero to the minimum uncut chip thickness (MUCT), while ploughing is paired to shearing for t_u ranging from MUCT to f_z. Furthermore, the determination of MUCT is crucial for the analytical model formulation.

MUCT can be calculated by considering how the Specific Cutting Force (SCF) peak changes by increasing the feed per tooth f_z. When ploughing is the dominant regime, the cutting process is interested by specific loads higher than expected one. MUCT can be considered equal to the minimum feed per tooth f_z from which the SCF peaks becomes constant. The cutting force F_c depends also on the chip section S, equal to the product between the depth of cut doc and chip thickness t_u. Therefore, the increase of f_z between two consecutive machining has a twofold effect on F_c. The SCF must be calculated by using Eq. 2 in order to highlight only the dependence of the cutting force on the deformation mechanism.

$$SCF(\theta) = \frac{Fc(\theta)}{doc * t_u(\theta)} \quad (2)$$

MUCT is a fundamental parameter of the analytical force model. The model computes the amount of material removed by a single tool tooth pass by considering the paths of the previous cutting edge and the current cutting edge. A cutting area A_c (see the square of Fig. 3) is calculated as the surface of the slice limited by the two cutting edge trajectories from 0° to ϑ, as expressed by Eq.3:

$$A_c(\theta) = \int_0^{\theta} \left(\frac{t_u(\theta) + t_u(\theta + d\theta)}{2} \right) R d\theta \quad (3)$$

where R indicates the tool radius.

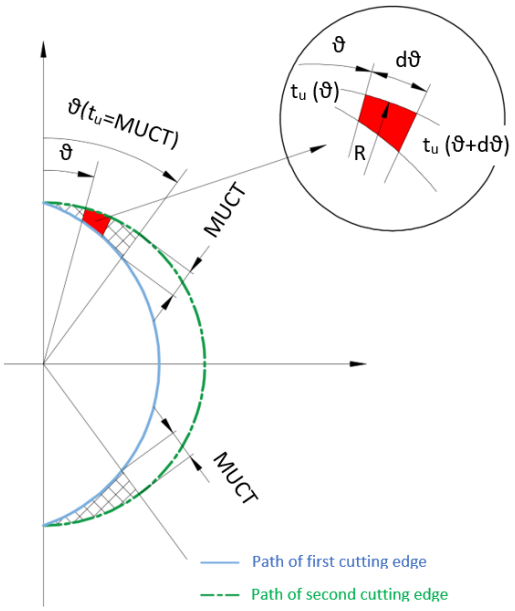

Fig. 3. A detailed view of the infinitesimal cutting area dA_C.

With the aim to consider the effect of ploughing on cutting force, a ploughed area A_p is defined as the portion of A_c which is elastically deformed instead of being cut. The Eq. 4 allows to compute A_p:

$$\begin{cases} if\ t_u(\theta) < MUCT\ and\ \theta < \Pi/2\ then\ A_p(\theta) = A_c(\theta) \\ if\ t_u(\theta) < MUCT\ and\ \theta > \Pi/2\ then\ A_p(\theta) = A_c(\pi) - A_c(\theta) \\ if\ t_u(\theta) > MUCT\ then\ A_p(\theta) = A_{pMAX} \end{cases} \quad (4)$$

The ploughed area A_p is equal to the cutting area A_c until t_u reaches the MUCT. The thickness t_u still increase since the angle ϑ reaches Π/2. When t_u is higher than MUCT, the area A_p remains constant until t_u decreases ($\vartheta > 90°$) and it reaches again the value of MUCT. The maximum ploughed area A_{pMAX} is equal to A_p when $t_u(\theta)$ is equal to MUCT. The ploughed area A_p is utilized to compute the tangential (F_t) and radial (F_r) components of the cutting force through Eq. 5 and Eq. 6:

$$F_t(\theta) = \left(K_{ts} * t_u(\theta) + K_{tp} * A_p(\theta)\right) * doc \quad (5)$$

$$F_r(\theta) = \left(K_{rs} * t_u(\theta) + K_{rp} * A_p(\theta)\right) * doc \quad (6)$$

Specific force parameters K_{ts} and K_{rs} are the shearing force coefficients in tangential and radial directions (N/mm^2) respectively, while parameters K_{tp} and K_{rp} are the ploughing force coefficients in tangential and radial directions (N/mm^3). The force coefficient values depend on the material properties and they should be determined through a refinement procedure based on the comparison between predicted and measured force components in x and y directions. The cartesian force components can be computed from F_t and F_r by using Eq. 7 and Eq. 8:

$$F_x = F_t * cos(\theta) + F_r * sin(\theta) \quad (7)$$

$$F_y = -F_t * sin(\theta) + F_r * cos(\theta) \quad (8)$$

$$F_c = \sqrt{{F_x}^2 + {F_y}^2} \quad (9)$$

4. Model calibration and results

Cutting force was measured during the preliminary micro slot machining to determine the MUCT. To statistically validate the procedure, a portion of signal which corresponds to thirty rotations of the micro tool was considered. The cutting force peak was computed for each rotation in order to calculate an average cutting force for each value of feed per tooth. The average cutting force peak was normalized on the chip cross section by using Eq. 2. Fig. 4 shows the relation between the specific cutting force and the feed per tooth. The specific load increment due to ploughing regime is clearly recognizable at low feed rate. As feed rate increases, the SCF generally decreases but the rate of decrease strongly reduces for feed per tooth greater than 2.5 µm/rev*tooth. In ploughing dominant region, the force data shows also a greater variability attributable to the higher instability compared to shearing. A value of 2.5 µm was utilized as MUCT in the subsequent analytical force model calibration.

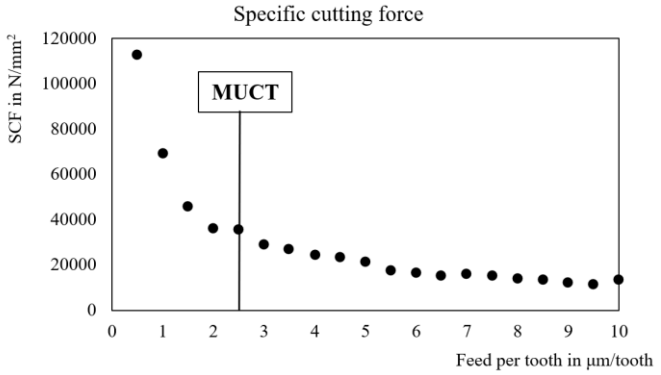

Fig. 4. Relation between the average peak of the specific cutting force and the feed per tooth

The model refinement consisted in the calculation of the best set of parameters K_{ts}, K_{rs}, K_{tp} and K_{rp} by minimizing the gap between the experimental cutting force and the model predictions. Cutting force were measured during the thin wall micro cuts summarized in Table 3. Average cutting force peaks were computed for each repetition of each machining test. The experimental data were utilized as benchmark for an iterative search artificial intelligence algorithm, the Particle Swarm Optimization (PSO) by Eberhart and Kennedy [20]. The objective function described in a previous research [21] was updated by considering the prediction error about the resultant cutting force F_c instead of the force components F_x and F_y. Furthermore, in [21] the model refinement was performed by considering only the test with the minimum force signal distortion due to tool run-out. The new objective function was computed as the sum of the prediction error of all the tests, as expressed by Eq. 10:

$$Objective\ Function = \sum \left(\frac{|F_{model.c\ MAX} - F_{exp.c\ MAX}|}{F_{exp.c\ MAX}} \right)_i \quad (10)$$

where $F_{model.c\ MAX}$ is the peak of predicted cutting for the i-th test, while $F_{exp.c\ MAX}$ is the average experimental peak of cutting force. Lower and upper bound were set in order to limit the parameters domain. The best solution was identified by using 150 particles after 1500 algorithm iterations and it is reported in Table 4 as optimum set with 2nd strategy.

Table 4. Bounds and optimum sets of the analytical model coefficients.

Parameter	Lower bound	Upper bound	Optimum set 1st strategy	Optimum set 2nd strategy
K_{ts}	0	10000	2595	1559
K_{tp}	0	5000	4625	2187
K_{rs}	0	10000	1870	2933
K_{rp}	0	5000	3000	4415

The optimum set computed by the 1st strategy of optimization is the results of the model tuning described in [21]. A comparison between the two strategies was performed in terms of percentage error of the model prediction for each repetition of each test. The result is expressed by Table 5, as an average prediction error calculated by considering the three repetitions of each test listed in Table 3.

Table 5. Average errors of the analytical model.

Test	Cutting speed (m/min)	Feed per tooth (µm/rev*tooth)	Average Error 1st strategy (%)	Average Error 2nd strategy (%)
1	30	2.5	2.5	-0.6
2	40	2.5	1.9	0.1
3	30	5	-10.4	-10.2
4	40	5	-12.4	-7.3
5	30	10	1.7	-0.3
6	40	10	0.9	1.3

The absolute values of percentage errors oscillate between 0.9 % and 12.4% with the model calibrated with first strategy, while the second strategy slightly improves the model accuracy. The percentage errors of the model calibrated by using the second strategy oscillate between 0.1% and 10.2%. Also with the new coefficient set, the model achieved the best results for Tests 1 and 2 and Tests 5 and 6. By considering a MUCT of 2.5 µm, Tests 1 and Tests 2 did not involve a transition of cutting regimes during the tool rotation. Ploughing was the unique and exclusive cutting regime, since the feed per tooth was equal to 2.5 µm/rev*tooth. At the same time, Tests 5 and Tests 6 were characterized by and early transition to shearing and the ploughing effect is neglectable. The model accuracy is maximum for tests in shearing and ploughing dominant region, while the accuracy reduces in intermediate cutting condition. Tests 3 and Tests 4 share a feed per tooth of 5 µm/rev*tooth. The transition from ploughing to shearing occurs at not-neglectable rotational angle of the tool edge.

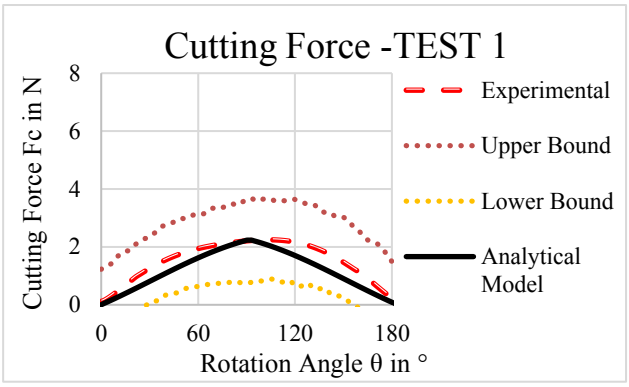

Fig. 5. Comparison between the experimental data and the model prediction for Test 1.

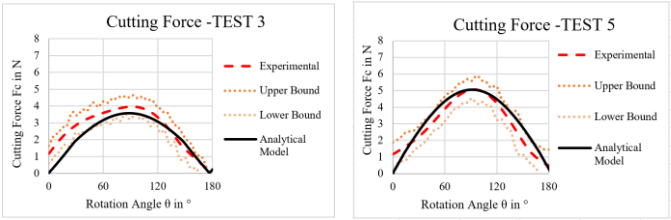

(a) (b)

Fig. 6. Comparison between the experimental data and the model prediction for Test 3 (a) and Test 5 (b).

Fig. 5 shows a comparison between experimental data and the model forecasting for Tests 1, while Fig. 6 illustrates the same comparison for Tests 3 (Fig. 6a) and for Tests 5 (Fig. 6b). Analogue data were achieved for Tests 2, 4 and 6, which were performed with the same feed rate but a higher cutting speed. The experimental data are presented with a confidence interval of 95%. Process variability appears meaningful in Tests 1 due to ploughing regime. The material is not correctly removed, but it is compressed and ploughed. Nevertheless, the model well fits the cutting force signal along the entire machining phase. The model is accurate also for Tests 5 in shearing dominant region. Fig. 6a shows as the model accuracy for Tests 3 is lower, but the model prediction is included in the confident region of the experimental data.

5. Conclusion

The authors investigated the micro-machinability of Inconel 625 samples formed by L-PBF process. The experimental analysis favorites the embedding between micro milling and additive manufacturing in order to integrate their respective advantages. An analytical model was successfully developed by considering the cutting regime transition, a key feature of micro machining processes. The Minimum Uncut Chip Thickness was experimentally determined, and it was utilized in the model tuning phase. Model calibration was approached by implementing an algorithm and by searching a best fit through the Particle Swarm Optimization technique. The model was subsequently applied to predict the cutting force, a fundamental process variable. A good matching between experimental data and model prediction was finally achieved as the major research output.

References

[1] Rinaldi S, Imbrogno S, Rotella G, Umbrello D, Filice L. Physics based modeling of machining inconel 718 to predict surface integrity modification. Procedia CIRP 2019,82:350-355.

[2] D'Addona DM, Raykar SJ, Narke MM. High speed machining of Inconel 718: tool wear and surface roughness analysis. Procedia CIRP 2017,62:269-274.

[3] Joshi SC, Sheikh AA. 3D printing in aerospace and its long-term sustainability. Virtual and Physical Prototyping 2015;10(4):175-185.

[4] Ford S, Despeisse M. Additive manufacturing and sustainability: an exploratory study of the advantages and challenges. Journal of Cleaner Production 2016,137:1573-1587.

[5] Schneider F, Das J, Kirsch B, Linke B, Aurich JC. Sustainability in ultra precision and micro machining: a review. International Journal of Precision Engineering and Manufacturing-Green Technology 2019,6(3):601-610.

[6] Altintas Y, Aslan D. Integration of virtual and on-line machining process control and monitoring. CIRP Annals 2017,66(1):349-352.

[7] Liu C, Li Y, Shen W. A real time machining error compensation method based on dynamic features for cutting force induced elastic deformation in flank milling. Machining Science and Technology 2018,22(5):766-786.

[8] Biró I, Szalay T, Geier N. Effect of cutting parameters on section borders of the empirical specific cutting force model for cutting with micro-sized uncut chip thickness. Procedia CIRP 2018,77:279-282.

[9] Iturbe A, Giraud E, Hormaetxe E, Garay A, Germain G, Ostolaza K, Arrazola PJ. Mechanical characterization and modelling of Inconel 718 material behavior for machining process assessment. Materials Science and Engineering 2017,682:441-453.

[10] Kuram E, Ozcelik B. Optimization of machining parameters during micro-milling of ti6al4v titanium alloy and inconel 718 materials using taguchi method. Journal of Engineering Manufacture 2015,231(2):228–242.

[11] Budak E, Ozlu E, Bakioglu H, Barzegar Z. Thermo-mechanical modeling of the third deformationzone in machining for prediction of cutting forces. CIRP Annals - Manufacturing Technology 2016,65(1):121–124.

[12] Moges TM, Desai KA, Rao PVM. Modeling of cutting force, tool deflection, and surface error in micro-milling operation. The International Journal of Advanced Manufacturing Technology 2018,98(9-12):2865-2881.

[13] Biondani FG, Bissacco G. Effect of cutting edge micro geometry on surface generation in ball end milling. CIRP annals 2019,68(1):571-574.

[14] Abeni A, Ginestra PS, Attanasio A. Micro-milling of Selective Laser Melted Stainless Steel. In Selected Topics in Manufacturing. Springer, Cham. 2020:1-12.

[15] Rodríguez P, Labarga JE. A new model for the prediction of cutting forces in micro-end-milling operations. Journal of Materials Processing Technology 2013,13:261–268.

[16] Chen W, Teng X, Huo D, Wang Q. An improved cutting force model for micro milling considering machining dynamics. International Journal of Advanced Manufacturing Technology 2017,93(9-12):3005-3016.

[17] Zhang X, Yu T, Wang W. Dynamic cutting force prediction for micro end milling considering tool vibrations and run-out. Proceedings of the Institution of Mechanical Engineers, Part C: Journal of Mechanical Engineering Science 2019,233(7):2248-2261.

[18] Abeni A, Lancini M, Attanasio A. Characterization of machine tools and measurement system for micromilling. Nanotechnology and Precision Engineering 2019,2:23-28.

[19] Abeni A, Ceretti E, Özel T, Attanasio A. FEM simulation of micromilling of CuZn37 brass considering tool run-out. Procedia CIRP 2019,82:172-177.

[20] Eberhart R, Kennedy J. A new optimizer using particle swarm theory. Proceedings of the Sixth International Symposium on IEEE 1995:39-43.

[21] Abeni A, Loda D, Özel T, Attanasio A. Analytical force modelling for micro milling additively fabricated Inconel 625. Production Engineering 2020,14(5):613-627.